Infrared Thermography Data Reduction Technique for Heat Transfer Measurements in the Boeing/AFOSR Mach-6 Quiet Tunnel

Mirko Zaccara*
University of Naples "Federico II", 80125 Naples, Italy

This paper describes an infrared (IR) thermography data reduction technique to estimate the convective heat flux over a sharp cone tested in the Boeing/AFOSR Mach-6 Quiet Tunnel in hypersonic flow. The infrared raw data are converted into temperature values by means of a radiometric calibration including the effect of the presence of the wind tunnel viewing window. The infrared directional emissivity of the model is considered. Temperature maps onto a 3D surface grid from 2D IR images are reconstructed by means of an optical calibration taking into account lens distortions. Model oscillations, due to sting mechanism vibrations, increase the temperature noise which is reduced with a single-step discrete Fourier transform approach. Convective heat flux is computed by means of an Inverse Heat Transfer Problem (IHTP). The 1D IHTP is solved and the experimental results are validated against the theoretical solution by performing runs with the cone at 0deg angle of attack with an average relative error of 3.6%. A 2D IHTP is developed to take into account tangential conduction caused by the crossflow vortices on the cone at 6deg angle of attack.

Nomenclature

Ch	=	modified Stanton number
c_p	=	specific heat at constant pressure
$\mathrm{d}t$	=	time step
E	=	error
F	=	modulation transfer function
$Fo_{\overline{\varpi}}$	=	modified Fourier number
f	=	residual, focal length
h	=	convective heat flux coefficient
k	=	thermal conductivity
M	=	Mach number
P	=	pressure
Pr	=	Prandtl number
q	=	heat flux
Re	=	Reynolds number
r	=	radius, recovery factor
r_i	=	upsampling factor
St	=	Stanton number
T	=	temperature
t	=	time
U	=	digital values, speed
α	=	thermal diffusivity
γ	=	specific heats ratio
ϵ	=	emissivity coefficient
ξ	=	arc length
ρ	=	density
σ	=	Stefan-Boltzmann constant

*Master Student, Department of Industrial Engineering, Aerospace Sector, Piazzale Tecchio 80; mirko.zaccara@libero.it

ψ	=	azimuth angle

Subscripts

0	=	stagnation value
∞	=	free-stream value
aw	=	adiabatic wall
c	=	convective
e	=	edge of the boundary layer
exp	=	experimental
num	=	numerical
i	=	initial
f	=	final
r	=	radiative, relative
th	=	theoretical
w	=	wall

I. Introduction

Heat flux measurements in the hypersonic regime are extremely important in several science and engineering problems such as the investigation of hypersonic laminar-to-turbulent transition which is crucial to lifting reentry vehicles, airbreathing cruise vehicles, and high-speed missiles [1, 2]. In fact, boundary layer state analysis is a key factor for the design of the thermal protection system and it deeply affects the skin friction, drag and moments [3, 4].
Conventional hypersonic wind tunnels have high levels of freestream fluctuations which are several orders of magnitude above flight levels. These freestream fluctuations are generally dominated by acoustic noise radiated from the turbulent boundary layers on the nozzle walls. The noise greatly affects the position and mechanism of laminar-turbulent transition on models [5]. This is why quiet flow wind tunnels, such as the BAM6QT, have been sought for more than 60 years. They provide uniform flow with noise level less than 0.10% allowing to collect data that can be related to flight [6].
Measurement of the convective heat flux is traditionally performed using heat flux sensors such as heated thin-foil, thin film sensors, and wall calorimeter [7]. When their application is not feasible, the surface heat flux distribution is obtained by solving an inverse heat transfer problem (IHTP) [8] starting from temperature measurements by means of thermocouples, resistance temperature detectors (RTDs) or infrared (IR) thermography. If the velocity and the temperature fields, and thus the heat flux distribution, exhibit very high spatial gradients, the heat flux evaluation, using zerodimensional sensors such as thermocouples or RTDs, can be troublesome [9, 10]. Instead, IR thermography is a non-contact technique which allows for accurate measurements of surface temperature maps . Compared to standard techniques, the use of IR technique has several advantages: it is non-intrusive and IR cameras have high sensitivity (up to 20 mK), fast response time (down to 20μs), and relatively high spatial resolution [11].
In this work, a data reduction technique to solve IHTPs starting from IR measurements is presented to evaluate convective wall heat transfer on a sharp cone in hypersonic flow. In Section II, the main features of the hypersonic quiet tunnel BAM6QT are described. The procedure to convert the raw IR data to 3D surface temperature map, considering lens distortions, model oscillations and model directional emissivity, is presented in Section III. In Section IV, the IHTP is presented while the obtained results are discussed in Section V and summarized in Section VI. In particular, this methodology has been applied to several experimental tests of a sharp cone tested in the BAM6QT at Mach number 6. The 1D IHTP is solved and the results are validated against the theoretical solution by performing runs with the cone at 0deg angle of attack as described in Section III. Schmidt-Boelter gauges and CFD simulations represented additional terms of comparison for the validation. A 2D IHTP has been implemented to take into account tangential conduction caused by the crossflow vortices on the cone at 6deg angle of attack. In these cases, measurement accuracy calculations have been conducted to check the 1D IHTP application and confirmed by the 2D IHTP results.

II. The Boeing/AFOSR Mach-6 Quiet Tunnel

The Boeing/AFOSR Mach-6 Quiet Tunnel is a facility at Purdue University in West Lafayette, Indiana-USA. Currently the BAM6QT is the biggest hypersonic quiet tunnel facility worldwide. A schematic of the tunnel is provided in Fig. 1. The BAM6QT is a Ludwieg tube design incorporating a long driver tube (37.3 m) connected to a converging-diverging nozzle to accelerate flow to Mach 6. Two burst diaphragms divide the facility into high and low pressure regions and they are positioned after the diffuser. This guarantees a reduction of disturbances in the test-section

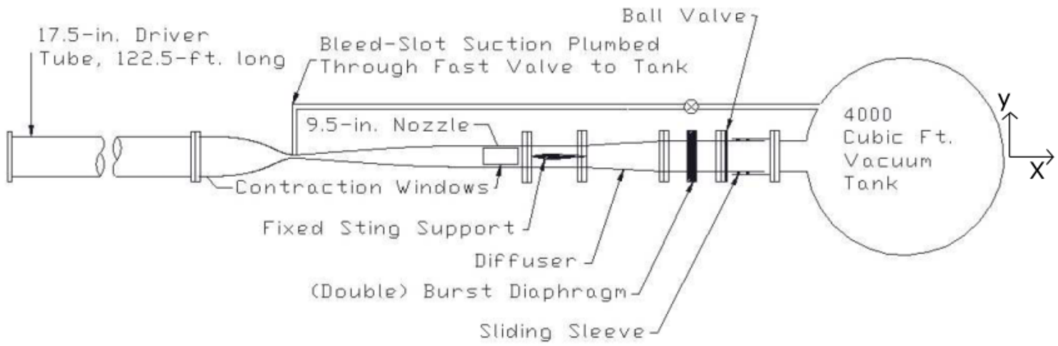

Fig. 1 Schematic of the Boeing/AFOSR Mach-6 Quiet Tunnel [6].

flow by producing a naturally low-noise acceleration from stagnation to nominal conditions. The test section consists in the aft part of the nozzle, where the cross-sectional area increases slowly and it is 241mm in diameter. The nozzle is very long to minimize the growth of the Görtler instability and it is highly polished to avoid roughness could lead to early transition. To help protect the mirror finish of the nozzle, a series of filters eliminate particles larger than 0.01μm from the air used to pressurize the driver tube. The BAM6QT viewing window is made of Calcium Fluoride CaF_2 covered with an anti-reflection layer to increase the transmissivity. It is transparent to radiations with a wavelength down to 7μm. Further details on the design of the facility are deeply discussed by Schneider [6]. The BAM6QT has some peculiar features to keep a laminar boundary layer on the nozzle wall to enable operation at low freestream noise levels less than 0.05%. Just upstream of the throat, a bleed-slot connected to the vacuum tank through a fast-opening butterfly valve is used to remove the wall boundary layer allowing a new laminar boundary layer to develop on the nozzle wall. If this slot is closed, the tunnel could be run noisy and the Mach number would be 5.8, since the turbulent boundary layer reduces the effective area ratio between the nozzle exit and the throat. When the desired pressure is reached in the driver tube, the air gap between the pair of diaphragms is evacuated and they are burst in quick succession. A shock wave and an expansion fan propagate downstream and upstream respectively. Once the expansion fan has passed through the throat, the air behind the expansion fan is accelerated through the nozzle at Mach 6. At present, the maximum stagnation pressure to obtain quiet flow conditions is 931 kPa. Since the driver tube is kept at 433K, the maximum unit Reynolds number related to quiet condition is $Re = 9.90 \cdot 10^6\ m^{-1}$. It is a common choice for Ludwieg tubes to end the run when the expansion wave that reflects at the upstream end of the driver tube reaches the contraction inlet again. For the BAM6QT, the time needed is 0.18s for $T_0 = 433$K. A Dan Tec hot-film sensor is installed on the nozzle wall to detect the turbulence level of the boundary level and a typical output is shown in Fig. 2a from which it is clear that the quiet flow conditions are reached ≈1s after the diaphragms burst (run starts in Fig. 2) and last about 2.5s. Data are collected with the presence of travelling expansion waves causing the stagnation pressure drop of 1% after each reflection in the driver tube. After a few reflections the fan spreads out and the thermodynamic quantities change nearly continuously dividing the run in different segments in which the mean thermodynamic conditions can be considered. As described later, the IHTP has been solved only in a time interval of 0.18s when the flow is quasi-static. In fact, as shown in Fig. 2b, the first part of the run is unsteady, the model experiences two sharp boosts of heat flux and therefore is not possible to define the IHTP because the convective heat transfer is time dependent.

III. Infrared Image Processing

In this paragraph, the steps involved in the approach to rebuild temperature maps onto a 3D surface grid from 2D IR images are described. Firstly, a radiometric camera calibration to convert IR raw data into temperature values is needed. Secondly, it is necessary to establish a correspondance between the points of the observed object and the pixels of the images by means of an optical camera calibration. Since the model oscillates, a correction is needed to reduce the data noise and assure to relate the temperature values always to the same pixel. Lastly, 3D temperature maps can be reconstructed by taking into account the directional emissivity of the model.

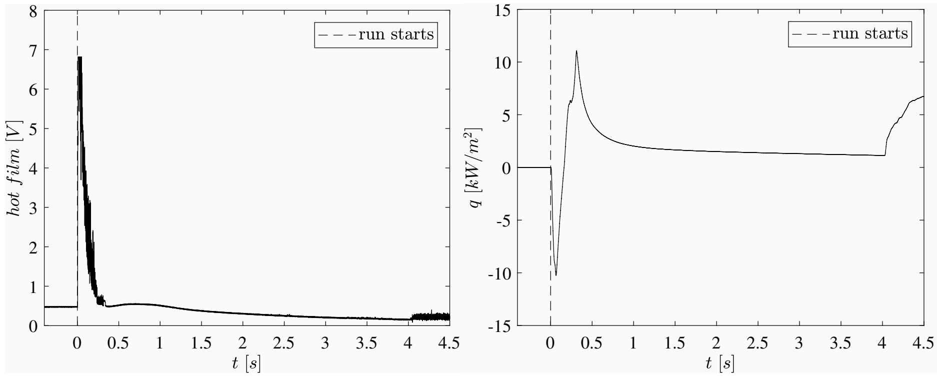

(a) Hot film output. (b) Schmidt-Boelter gauge output.

Fig. 2 Typical hot film output and convective heat transfer on the model for a BAM6QT quiet flow run.

A. Radiometric Calibration

A radiometric camera calibration is necessary to convert the output signal of the IR camera to the real viewed object temperature. Most modern cameras like the Infratec imageIR® 8300 hp, used for the present work, are already calibrated for a different number of integration times that give accurate output in an established temperature measurement range. However, the factory calibration is not accurate when a viewing window is present in the optical path. Since the window absorbs part of the radiation, it is expected that the factory calibration would underrate the temperature values. The IR camera radiometric calibration has been conducted by using a black body [7]. It is advisable to calibrate the IR camera by using the actual optical path employed in the experimental tests, which means having the black body in the test section and the camera looking at it through the viewing window. Unfortunately, this configuration was considered not feasible in the BAM6QT because of a possible contamination of the nozzle polishing. As a consequence, the calibration has been conducted outside the wind tunnel by respecting the model - window - camera distances and therefore taking into account the viewing window transmissiviy. A total of 28 infrared images of the black body have been collected for a temperature range from 10°C to 50.5°C. The calibration resulted in a temperature accuracy of ±0.08K.

B. Optical Calibration

The two-dimensional temperature map detected by an infrared camera is the planar projection of the thermal field which is viewed in the physical three-dimensional space. Since the tested model is not planar, an optical calibration to have a correspondance between the image and the real world coordinate systems is needed. The approach proposed by Cardone et al. [11] is used. The method uses a camera model that is based on a combination of linear and nonlinear techniques using a perspective projection model, named as the pinhole model, augmented with a correction for lens distortions [12]. The employed calibration target is an aluminum plate with a grid of regularly spaced drilled holes. Due to the symmetry of circular markers, a detection scheme is easy to implement as well as robust in off-axis or rotated viewing arrangements. The target was moved along the volume occupied by the tested model. In this way, more images of the target were taken and the whole observed volume was mapped. The markers appear as hot spots on a cold surface thanks to the low emissivity of the aluminum plate. The positions of the markers are found within the IR images as the barycentre of the hot regions and their position are used to determine the camera calibration constants. As proposed by Heikkilä [12], a Direct Linear Transformation (DLT) is used to produce the first constants estimation by considering the optical centre as the centre of the square sensor and no lens distortions with the ideal focal length. The calibration constants are then found by minimizing the root mean square residual between the known image coordinates of the control points and their image coordinates computed in accordance with the camera model. The minimization process is performed with Levenberg–Marquardt method [13]. In the present work, only three planes have been used for the optical calibration to map the whole volume occupied by the model with a coefficient of determination $R^2 = 0.999$.

C. Model Oscillation

In order to complete the image registration procedure, model oscillations must be taken into account to assure that they do not affect the time history map used in the IHTP. For the BAM6QT, the main reason of model movements is the

burst of the diaphragms at the beginning of the run, which makes the whole tunnel oscillate. Actually, the burst mainly causes oscillations of the model along tunnel x-axis, while they are small along y-axis and z-axis. As a consequence, the in-plane displacements are represented by 2D rigid translations and the out-of-plane displacements are not considered. The image registration algorithm used in the present work is the single-step Discrete Fourier Transform (DFT) proposed by Manuel Guizar-Sicairos et al. [14]. The proposed method reduces computational load and memory requirements without sacrificing accuracy. The IR image at $t = 0.5$s has been chosen as reference image to compute the model displacements moving forward from $t = 0.5$s. Actually, moving backward from $t = 0.5$s, the corrected previous image is used as a reference for the next one. In fact, as shown in Fig. 2b, the model experiences two sharp boosts of heat flux which deeply change the measured digital values. As a consequence, each image is too different to the reference one at $t = 0.5$s to give good results.
The image registration process is based on two steps. An initial estimate of the location of the cross-correlation peak between the investigated image and the reference one to compute the displacements is obtained by the FFT method with an upsampling factor of $r_i = 2$ [13]. The second step refines the location of the peak location, to within a desired fraction of a pixel, by means of matrix multiplication of the 2D DFT [15].
In the single-step DFT algorithm, an upsampled cross-correlation (by a factor r_i) is computed in a 1.5×1.5 pixel neighborhood about the initial estimate. For the 512×640 pixels camera used in this work, the computational load with $r_i = 10$ is of order of magnitude $4.5 \cdot 10^8$ for the FFT approach and $3.3 \cdot 10^6$ with this more efficient method. Typical model displacements evaluated during the run are shown in Fig. 3. While along the y-axis the displacements is only of nearly 5 pixels, along x-axis it is larger than 30. This is why it is extremely important to correct for these oscillations.

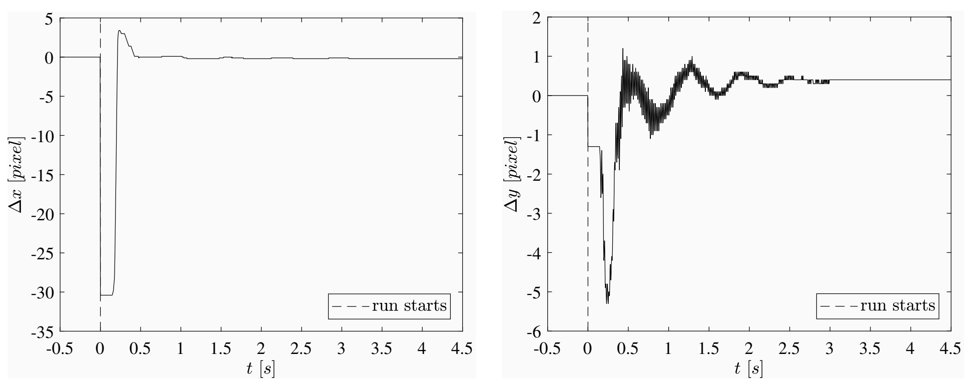

(a) Displacement along x.

(b) Displacement along y-axis.

Fig. 3 Typical model displacements during the run.

D. 3D Surface Temperature Maps

The first step of 3D temperature map reconstruction is the generation of the mesh on the model surface. The mesh spacing has to be chosen to be just slightly higher than the spatial resolution of the IR camera, to avoid both loss of information and useless extra points, which would only increase the computational load. The previously computed camera model constants are used to establish a correspondence between the points of the mesh and the pixels of the IR image. As a result, it is possible to project the mesh points on the IR images. Actually, the mesh points do not correspond with the centers of the pixels so the digital values acquired by the IR camera need to be interpolated.
At this point, the viewing angle θ on the object surface can be easily evaluated as the scalar product between the viewing ray direction and the known normal unit vector of the model surface [11]. Then, the model emissivity can be corrected with a law that relates it to the viewing angle [16, 17]. Eventually, as described by Cardone et al. [11], the temperature for each grid point can be evaluated and an example of 3D surface temperature maps is shown in Fig. 4.

IV. Inverse Heat Transfer Problem

Inverse Heat Transfer Problems are applied to estimate the convective wall heat flux in high-speed flows to better understand physical phenomena like boundary-layer transition, shock-boundary layer interaction, and flow separation. An overview of heat flux estimation methods is provided by Walker and Scott [8] who demonstrated the necessity of

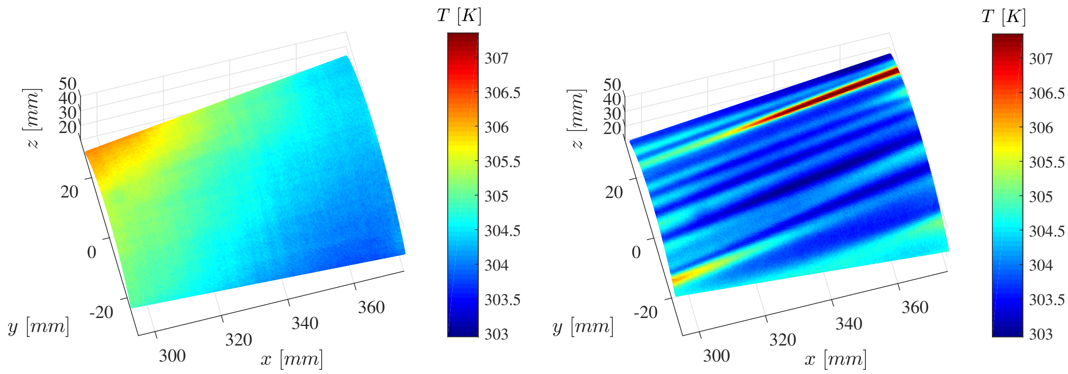

(a) 0 deg angle of attack.

(b) 6 deg angle of attack.

Fig. 4 Examples of 3D temperature maps reconstruction of the cone surface under analysis.

solving IHTPs instead of direct methods especially when dealing with high unsteady heat flux and strong temperature gradients. The IHTP is classified as an ill-posed problem: the solution is not unique and it can considerably vary with small changes in input data caused by measurements and modelling errors [18]. An overview of the IHTP past applications and resolution methods is provided by Avallone et al. [19, 20].

In the presence of phenomena characterized by strong temperature gradients, it may be necessary to solve a multidimensional full inverse heat transfer problem. It is necessary to define the boundary conditions adopted for the heat equation as follows (see Fig. 5 for the sketch of a generic 3D problem):

$$\begin{cases} k\nabla^2(T) = \rho c_p \frac{\partial T}{\partial t} & \\ T(x,y,z,0) = T_{w,i} & \text{at } t=0 \\ T(x,y,z,t) = T_{w,i} & \text{at } z \in F,\ \forall t \in \left[0, t_f\right] \\ T(x,y,z,t) = T_w & \text{at } z \in S,\ \forall t \in [0, t_i] \\ k\left.\frac{\partial T(x,y,z,t)}{\partial n}\right|_S = q_w(x,y,t) & \text{at } z \in S,\ \forall t \in \left[t_i, t_f\right] \end{cases} \tag{1}$$

Here, k is the thermal conductivity, ρ is the model material density, and c_p is the specific heat of the material assumed constant in Eq. (1). The time interval of interest described in the following is identified by t_i and t_f. The initial temperature distribution is assumed to be constant in the entire domain and equal to the surface temperature $T_{w,i}$ which is known from the infrared measurements. The first boundary condition is to consider the wall F to be isothermal. This assumption is valid if the thickness of the material is larger than the penetration depth [21].

The second boundary condition is chosen in relation to the moment of the run. Since the decrease of the stagnation quantities in the tunnel is nearly continuous, it has been straightforward chosen to calculate the heat flux in a small time interval of interest of $\Delta t = 0.18$s after the quiet flow conditions are reached ($t > 1$s). Within the time interval of study, mean values of the thermodynamic quantities and Reynolds number are considered. For this time interval the boundary condition is represented by the unknown heat flux $q_w(x,y,z,t)$ on the surface exposed to the flow (S). The heat flux can be expressed as a function of the convective and radiative heat transfer:

$$\begin{aligned} q_w(x,y,z,t) = k\left.\frac{\partial T(x,y,z,t)}{\partial n}\right|_S = h(x,y,z)\left(T_{w_{num}}(x,y,z,t) - T_{aw}\right) + \\ +\sigma\epsilon_t\left(T^4_{w_{num}}(x,y,z,t) - T^4_r\right) \qquad \text{at } z \in S \end{aligned} \tag{2}$$

The heat flux $q_w(x,y,z,t)$ at $z \in S$ depends on the convective heat transfer coefficient h which is the only unknown and needs to be estimated. When considering a short duration interval one can assume that the convective heat transfer coefficient remains constant and time-independent. This assumption can be made in the BAM6QT because the surface temperature rise is relatively small with respect to the adiabatic wall temperature T_{aw} and thus the boundary layer characteristics do not vary. In Eq. (2), $T_{w_{num}}$ is the transient wall temperature that, in the following, is obtained from the transient heat conduction equation Eq. (1); T_{aw} is the adiabatic wall temperature calculated either from the laminar

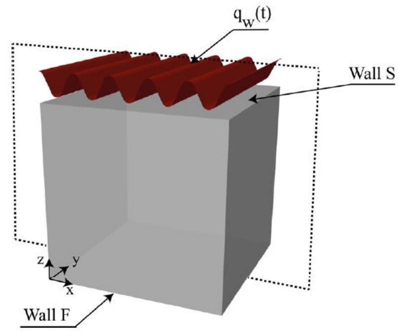

Fig. 5 Sketch of a generic 3D model adapted from [20].

boundary layer theory or chosen to be equal to the stagnation temperature T_0; ϵ_t is the total emissivity chosen to be equal to the normal surface emissivity in the infrared band studied; σ is the Stefan–Boltzmann constant, and T_r is the enclosure temperature towards which the model radiates. In practice, in cold wind tunnel applications like the BAM6QT, T_r is coincident with the ambient temperature [22].
The IHTP is solved by means of a recursive least-square approach in the time interval of interest. It works by varying the unknown parameter h in order to minimize the residual $f\left(\underline{h}\right)$ between the measured temperature Tw_{exp} and $T_{w_{num}}$ generated by solving the heat equation Eq. (1):

$$f\left(\underline{h}\right) = \int_{t_i}^{t_f} \left[T_{w_{exp}}\left(\underline{x}, t, \underline{h}\right) - T_{w_{num}}\left(\underline{x}, t, \underline{h}\right)\right] dt \tag{3}$$

Due to the long tunnel startup and the unsteady part of the run, before the time interval of study, the boundary condition $T\left(x, y, z, t\right) = T_w$ is applied to numerically solve the Direct Heat Transfer Problem (DHTP). This guarantees that the temperature state within the spatial mesh is a correct initial condition for the time interval of interest $[t_i, t_f]$ in which the convective heat transfer coefficient h is evaluated. In the optimization procedure, the convergence is reached if, between two subsequent iterations, both the step sizes $\underline{\Delta h}$ and $f\left(\underline{h} + \underline{\Delta h}\right) - f\left(\underline{h}\right)$ are lower than 10^{-6}.

V. Experimental Data

A. Experimental Apparatus

The experimental tests have been carried out in the Boeing/AFOSR Mach-6 Quiet Tunnel described in Section II. The IR thermography measurements are performed using the Infratec imageIR® 8300 hp. The camera has a Mercury Cadmium Telluride (MCT) quantum detector array of 640 × 512 pixels and a spectral range of 2.0 - 5.7μm. The camera is operated at 300Hz to have enough frames to better dicretize the unsteady flow. The integration time was set to 1290μs to increase the measurements accuracy. A wide-angle lens has been used with a focal length of 12mm and a field of view FOV of 43.6deg × 35.5deg. The camera was rotated with respect to the viewing window normal to prevent for self-reflection and it was shielded with black paper to prevent spurious reflections from the background and window.
The wind tunnel test model is a 7° half-angle sharp, circular cone 406mm long founded on a modular concept [23] shown in Fig. 6a. A polyether ether ketone (PEEK) sensor frustum (Fig. 6b) has been used for infrared measurements. This element starts at $x = 247$mm distance from the nosetip and ends at $x = 385$mm, where x is along the tunnel axis of symmetry. When performing runs at 0deg angle of attack, three Schmidt-Boelter gauges have been hosted in the sensor frustum holes to have local heat flux measurements for the validation.

B. 1D Data Reduction Results and Validation

In order to validate the Infrared data reduction technique developed, some runs with the cone at 0 deg angle of attack have been conducted. The Reynolds number on the PEEK is sufficiently low to assure a laminar boundary layer ($Re < 10^7$). Since the flowfield is completely axisymmetric, a one-dimensional model of the problem Eq. (1) has been solved using a finite difference approach. In particular, a backward Euler implicit scheme has been implemented for the time integration because it is absolutely stable and second order accurate in space and time [24]. The domain depth was assumed equal to 5mm to have margin of safety since the penetration depth was found to be 3.84mm. The time step dt was forced to be equal to the one between two subsequent IR images.

(a) The model on the wind tunnel sting. (b) PEEK sensor frustum overview.

Fig. 6 Wind tunnel test model.

In the following, the Stanton number St is used as non-dimensional parameter to discuss the experimental results related to the convective heat flux q_c.

$$St = \frac{q_c}{c_{p_\infty}\rho_\infty U_\infty \left(T_{aw} - T_w\right)} \tag{4}$$

In Eq. (4) the parameters T_w, c_{p_∞}, ρ_∞ and U_∞ are respectively the wall temperature and the free-stream constant-pressure specific heat, flow density, and speed. The definition of the adiabatic wall temperature T_{aw} for a laminar boundary layer is taken from Shapiro [25]:

$$T_{aw} = T_e\left(1 + \frac{\gamma - 1}{2} r M_e^2\right) \tag{5}$$

where T_e and M_e are the static temperature and Mach number at the edge of the boundary layer respectively. The recovery factor r was considered equal to $\sqrt{Pr}$ (flat plate) being a reasonable approximation.
As already said, the IHTP has been solved in a time interval of 0.18s. Its position during the run time is found by fixing a Reynolds number per unit arc length ξ ($Re/\xi = \rho_\infty U_\infty/\mu_\infty$) which decreases during the run because of the drop of P_0 and T_0. For each run, the experimental solution has been directly compared and validated against the theoretical laminar solution for the cone. The latter has been evaluated as proposed by Sullivan and Liu [26] using both a similarity solution and a reference temperature method. The conditions at the edge of the boundary layer are evaluated from the Taylor-Maccoll theory. In order to have additional terms of comparison, three Schmidt-Boelter gauges have been installed on the model to have local measurements of convective heat flux. Moreover, a computational fluid dynamics (CFD) analysis has been conducted per each run using a two-dimensional solver named STABL2D [27].
A total of 19 runs have been performed with the cone at 0deg angle of attack. Different free-stream conditions have been tested to have a wide range of data for the validation of the data reduction technique. The results are summarized in Fig. 7. The experimental results from IR measurements show exceptional agreement with the theoretical solution. The IR measurements relative error $E_r = |St_{th} - St_{exp}|/St_{th}$ has been evaluated for five Reynolds number for a total of 67 values as a statistical population. The results are shown in Fig. 8a. The average error is $\approx 3.6\%$ and it is an excellent results when compared with the Schmidt-Boelter gauges errors shown in Figure 8b with an average error of about 28%, 40% and 47% for SB1, SB2 and SB3 respectively. As can be noticed in Fig. 7, the CFD computations show a constant error of 5%. For $Re = 2.68 \cdot 10^6$ the Stanton number has been evaluated for each run and the normalized standard deviation has been found to be 4.35% which is promising for future works.

C. 2D Data Reduction Results

Several runs with the cone at 6deg angle of attack have been performed. Due to the spanwise temperature gradients caused by the crossflow vortices, a two-dimensional inverse heat transfer problem has been solved to take into account tangential conduction. In particular, a 2D heat equation in cylindrical coordinates (r, ψ, x) for a fixed x has been solved using a backward Euler implicit scheme with a finite difference approach. The domain has been discretized using a number of elements on the boundary surface with the same spatial resolution of the mesh grid used for the temperature map reconstruction with a depth of 5mm. A trust-region reflective algoritm is used for the residual optimization (Eq. (3)) and the computational costs are reduced by means of a discrete fourier transform (DFT) iterative procedure proposed by Avallone et al. [20]. The relevance of the tangential conduction is quantified by means of the Modulation Transfer

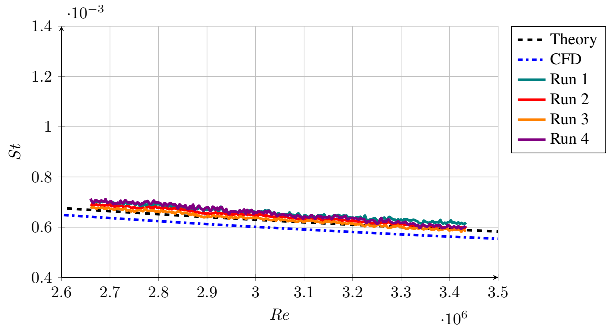

(a) $P_{0,i} = 910\ kPa, T_{0,i} = 426\ K, Re/\xi = 9.60 \cdot 10^6 \mathrm{m}^{-1}$.

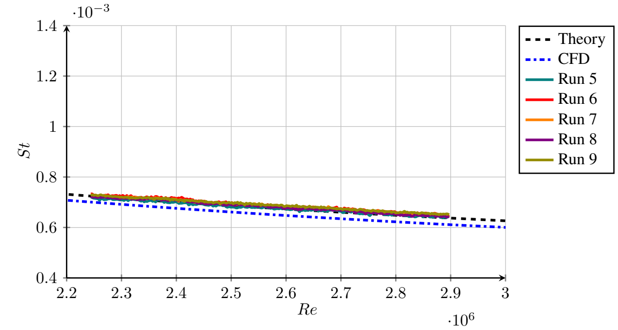

(b) $P_{0,i} = 807\ kPa, T_{0,i} = 428\ K, Re/\xi = 8.10 \cdot 10^6 \mathrm{m}^{-1}$.

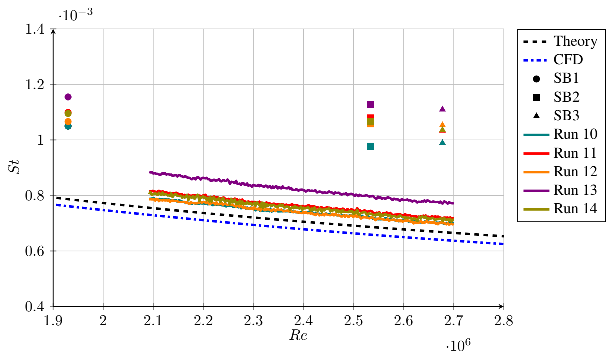

(c) $P_{0,i} = 745\ kPa, T_{0,i} = 426\ K, Re/\xi = 7.55 \cdot 10^6 \mathrm{m}^{-1}$.

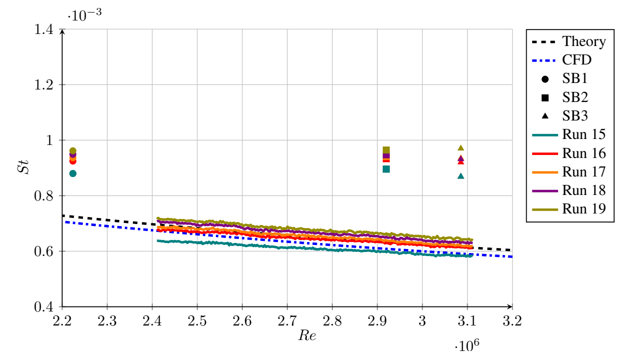

(d) $P_{0,i} = 876\ kPa, T_{0,i} = 429\ K, Re/\xi = 8.70 \cdot 10^6 \mathrm{m}^{-1}$.

Fig. 7 Experimental and theoretical results comparison.

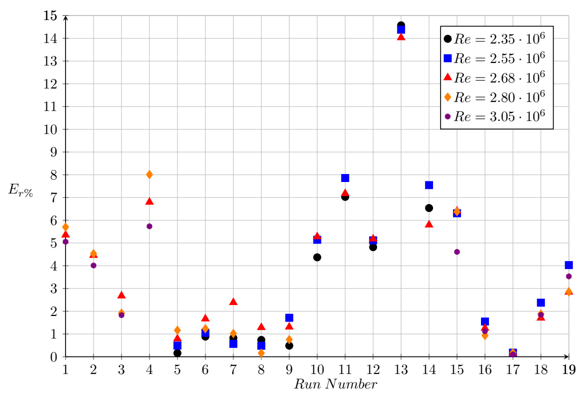

(a) IR measurements error.

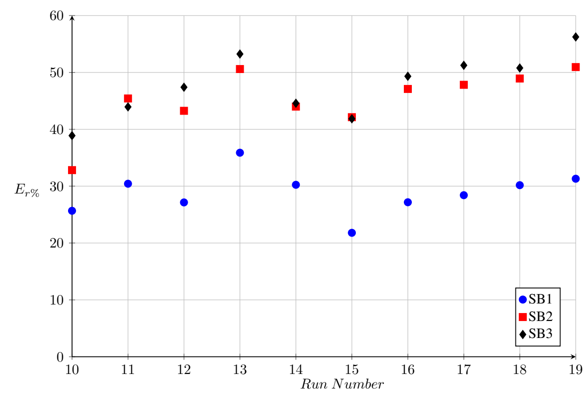

(b) SB gauges measurements error.

Fig. 8 Measurement errors of (a) IR technique and (b) SB gauges against the theoretical solution.

Function F [7] based on the modified Fourier number $Fo_{\overline{\omega}}$ evaluation. For the present work, a value of F=0.958 is found which means a predicted modulation of 4.2% in terms of peak to valley difference between the 1D and 2D solution.
In the following, the results are shown in terms of Modified Stanton number Ch which is defined as Eq. (4) but the stagnation temperature T_0 is used instead of the adiabatic wall temperature T_{aw} not available in this condition. The raw temperature data have been filtered by a second order polynomial space-time filter to reduce the random measurement noise. The 1D results are used as first guess for the 2D optimization process to accelerate the convergence to the solution. The latter is obtained by optimizing 39 coefficients of the DFT (30% of the total) that contribute to the 97% of the total power spectral density. The Ch measured with the 2D approach is compared to the 1D solution in Fig. 9.
Due to the favourable thermal properties of the PEEK ($\alpha = 2.17 \cdot 10^{-7} \mathrm{m}^2/\mathrm{s}$ and $\epsilon = 0.91$), the experiment carried out is

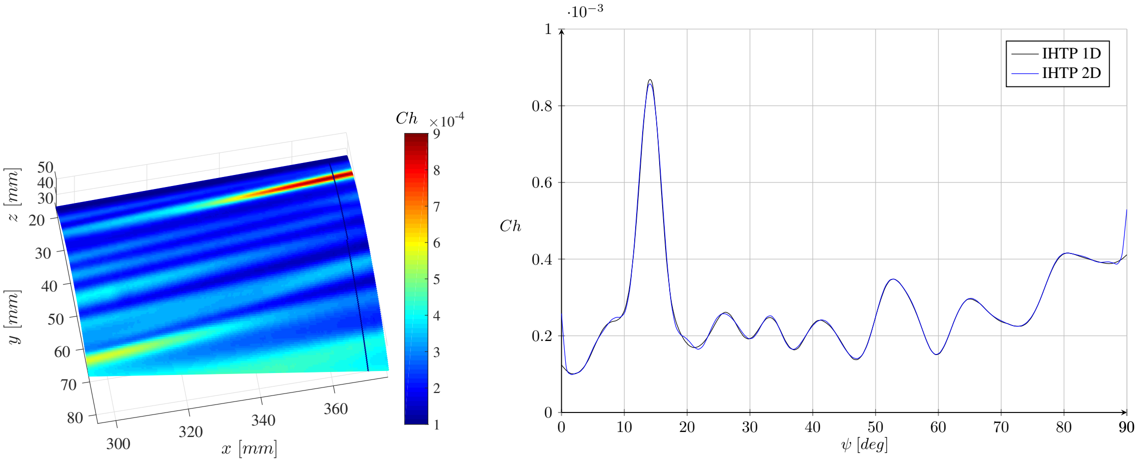

(a) 1D Stanton map. (b) 1D and 2D solution comparison.

Fig. 9 Spanwise modified Stanton-number distribution along the black line shown in the 1D map (a) from the 1D and 2D technique. Cone at 6deg angle of attack, $P_{0,i}$ = 762 kPa, $T_{0,i}$ = 429 K, $Re/\xi = 7.72 \cdot 10^6$ m^{-1}.

weakly affected by the tangential conduction. As a matter of fact, Figure 9b shows a difference between the 1D and 2D estimation lower than 5% which is perfectly in agreement with the predicted value except for some effects due to the inverse technique uncertainty and the DFT application at the two boundaries (ψ = 0deg and ψ = 90deg).

VI. Conclusion

An infrared thermography data reduction technique to solve 1D and 2D Inverse Heat Transfer Problem (IHTP) is presented. Firstly, the camera calibration has been conducted to incorporate the transmissivity of the wind tunnel viewing window. The infrared raw data are then converted to temperature values with a residual error of ±0.08K. The infrared directional emissivity of the model material has been taken into account to correct the temperature data and increase the results accuracy. IR images have been recorded using a camera model based on perspective projection approach taking into account lens distortions. The optical calibration has been conducted with a coefficient of determination $R^2 = 0.999$. An image registration algorithm has been used to correct for model oscillations. The approach based on the single-step DFT seems to be very useful to reduce noise with a subpixel accuracy. Eventually, three-dimensional maps of temperature have been presented. The 1D IHTP has been developed and validated by performing runs with the cone at 0deg angle of attack. The results have been compared with the theoretical solution in terms of Stanton number showing exceptional agreement with an average error of 3.6% and a normalised standard deviation of 4.35%. The experimental results are absolutely promising for future works especially when compared with the Schmidt-Boelter gauges measurements whose error is higher than 22% and with the CFD computations error of 5%. The 2D IHTP has been developed to take into account tangential conduction caused by the crossflow vortices on the cone tested at 6deg angle of attack. The computational cost is reduced by optimizing only 39 coefficients (30% of the total) of the discrete Fourier decomposition of the convective heat flux coefficients vector. For the present work, the one-dimensional technique has been found to modulate the convective heat flux of 4% according the Modulation Transfer Function theory. The two-dimensional analysis showed a modified Stanton number modulation of 5% in respect with the 1D measurements which is in accordance with the predicted value. This error can be considered acceptable for future works and the application of the two-dimensional model should be checked in terms of computational cost feasibility.

References

[1] Tony C. Lin, Wallis R. Grabowsky, and Kevin E. Yelmgren. "The search for optimum configurations for re-entry vehicles". J Spacecr Rockets, 21(2):142–149, March-April 1984.

[2] Steven P. Schneider." Laminar-Turbulent Transition on Reentry Capsules and Planetary Probes". J. Spacecr. Rockets, 43(6):1153–1173, November-December 2004.

- [3] H. Legner, A. Gelb, D. Rosen, and G. Caledonia." High velocity interceptor investigations". Technical Report PSI-1239/TR-1573, Physical Sciences Inc., September 1998. DTIC citation AD-A357979.
- [4] John D. Anderson, Jr., *Hypersonic and high temperature gas dynamics*, McGraw-Hill, Boston, Massachusetts, 1989.
- [5] Steven P. Schneider." Effects of high-speed tunnel noise on laminar-turbulent transition". J. Spacecr. Rockets, 38(3):323-333, May-June 2001.
- [6] Steven P. Schneider. "Development of Hypersonic Quiet Tunnels". J. Spacecr. Rockets, 45(4):641-664, July-August 2008.
- [7] Astarita T., Carlomagno GM., *Infrared thermography for thermo-fluidynamics*. Berlin Heidelberg, New York (USA), 2013.
- [8] Walker DG., Scott EP., "Evaluation of estimation methods for high unsteady heat fluxes from surface measurements". J. Thermophys. Heat Transfer. 1998;12(4):543–51.
- [9] de Luca L, Cardone G. "Modulation transfer function cascade model for a sampled IR imaging system". Appl. Opt. 1991;30(13):1659–64.
- [10] Schrijer FFJ. "Unsteady data reduction techniques for QIRT: consideration of temporal and spatial resolution". QIRT Conference 2012; Naples, Italy. Available at QIRT Open Archives: `http://www.qirt.org/dynamique/index.php?idD=60`. Paper QIRT 2012-317.
- [11] Cardone, G., Ianiro, A., dello Ioio, G. et al. *Temperature maps measurements on 3D surfaces with infrared thermography* Exp. in Fluids (2012) 52:375. DOI:10.1007/s00348-011-1225-9
- [12] Heikkilä J, Silven O (1997), "A four-step camera calibration procedure with implicit image correction". Proceedings of the 1997 conference on computer vision and pattern recognition (CVPR '97): 1106–1112
- [13] Marquardt D (1963),"An algorithm for least-squares estimation of nonlinear parameters". SIAM J Appl Math 11(2):431–441
- [14] Guizar-Sicarios M, Thurman ST, Fienup JR., "Efficient subpixel image registration algorithms". Opt. Lett. 2008;33(2):156–8.
- [15] H. H. Barrett and K. J. Myers, *Foundations of Image Science* (Wiley, 2004), p. 172.
- [16] Siegel R, Howell JR (1992), *Thermal Radiation Heat Transfer*, 3rd edn. Hemisphere, Washington
- [17] Ianiro A, Cardone G (2010), "Measurement of surface temperature and emissivity with stereo dual-wavelength IR thermography". J Mod Opt 57(18):1708–1715
- [18] Beck JV, Blackwell B, Clair CRS. *Inverse Heat Conduction: ill-posed problems*. New York (NY): Wiley Interscience; 1985.
- [19] Avallone F., Greco C., S.and Ekelschot D., (2013), "Image resection and heat transfer measurements by IR thermography in hypersonic flows", Quant. Infr. Therm. J., 10(2):188-206, DOI: 10.1080/17686733.2013.800697
- [20] Avallone, F., Greco, C. G., Schrijer, F. F. J. and Cardone, G. (2015), "A low-computational-cost inverse heat transfer technique for convective heat transfer measurements in hypersonic flows", Exp. in Fluids, 56(4) DOI: 10.1007/s00348-015-1951-5
- [21] Schultz DL, Jones TV (1973), "Heat-transfer measurements in short duration hypersonic facilities". NATO Advisory Group for Aerospace Research and Development, 165
- [22] Gülhan A, Schütte G, Stahl B (2008), "Experimetnal study on aerothermal heating caused by jet-hypersonic crossflow interaction". J. Spacecr. Rockets 45(5):891–899
- [23] Chynoweth B. C., Edelman J. B., Gray K.A., McKiernan G.R. and Schneider S. P., "Measurements in the Boeing/AFOSR Mach-6 Quiet Tunnel on Hypersonic Boundary-Layer Transition", 47th AIAA Fluid Dynamics Conference, AIAA AVIATION Forum, (AIAA 2017-3632)
- [24] LeVeque, R. (2007), *Finite Difference Methods for Ordinary and Partial Differential Equations*, Society for Industrial and Applied Mathematics, DOI: 10.1137/1.9780898717839
- [25] Shapiro A. H., *The dynamics and thermodynamics of compressible fluid flow*, The Ronald Press Company, New York 1953
- [26] Liu T, Wang B, Rubal J, Sullivan JP (2011), "Correcting lateral heat conduction effect in image-based heat flux measurements as an inverse problem". Int. J. Heat Mass Transfer, 54(5-6): 1244-1258.
- [27] Johnson H., Candler G. and Alba C., "Three-Dimensional Hypersonic Boundary Layer Stability Analysis with STABL-3D".U.S. Air Force Research Laboratory, University of Minnesota, 40th Fluid Dynamics Conference and Exhibit Chicago, Illinois